agriculture

MDPI

Article

Unmanned Aerial Vehicle-Based Techniques for Monitoring and Prevention of Invasive Apple Snails (*Pomacea canaliculata*) in Rice Paddy Fields

Senlin Guan [1,*], Kimiyasu Takahashi [1], Shunichiro Watanabe [2] and Katsunori Tanaka [2]

[1] Division of Crop Rotation Research for Lowland Farming, Kyushu-Okinawa Agricultural Research Center, National Agriculture and Food Research Organization, 496 Izumi, Fukuoka 833-0041, Chikugo, Japan
[2] Nileworks Co., Ltd. 2F, Kanda Square Front, 1-4-3 Kanda Nishikicho, Chiyoda, Tokyo 101-0054, Japan
* Correspondence: guan.s@affrc.go.jp; Tel.: +81-942-52-0692; Fax: +81-942-53-7776

Abstract: The destructive impact of invasive apple snail (*Pomacea canaliculata*) on young rice seedlings has garnered global attention, particularly in warm regions where rice production occurs. The preventative application of insecticide, particularly in areas with young rice seedlings and water depths exceeding 4 cm, has proven effective in mitigating this damage. In line with this recommendation, our study investigates the efficacy of site-specific drone-based insecticide applications to mitigate snail damage in rice paddies. These site-specific drone applications were strategically executed as directed by a highly accurate prescription map indicating the required insecticide quantity at specific locations. The prescription map was automatically generated through an advanced data processing program that used the aerial images acquired by a Real-Time Kinematic (RTK)-Unmanned Aerial Vehicle (UAV) as the input. Criteria were established to select the treatment locations; a value of below 4 cm from the top 95% percentile in the histogram of ground elevation data was used as a threshold to identify areas with a high-density of snail damage. The results demonstrated reductions in both the rates of rice damage and chemical usage following site-specific drone applications compared with the control fields. The findings in this study contribute to the advancement of effective site-specific pest control in precision agriculture.

Keywords: unmanned aerial vehicle; remote sensing; apple snail; *Pomacea canaliculata*; site-specific application; drone-based application

Citation: Guan, S.; Takahashi, K.; Watanabe, S.; Tanaka, K. Unmanned Aerial Vehicle-Based Techniques for Monitoring and Prevention of Invasive Apple Snails (*Pomacea canaliculata*) in Rice Paddy Fields. *Agriculture* **2024**, *14*, 299. https://doi.org/10.3390/agriculture14020299

Academic Editors: Gniewko Niedbała, Sebastian Kujawa, Magdalena Piekutowska and Tomasz Wojciechowski

Received: 15 January 2024
Revised: 8 February 2024
Accepted: 10 February 2024
Published: 13 February 2024

1. Introduction

The invasive apple snail (*Pomacea canaliculata*), recognized as one of the world's 100 most invasive alien species in the International Union for Conservation of Nature's list [1]. It has extensively invaded agricultural and natural ecosystems in numerous moderate-temperature regions across the globe [2]. *P. canaliculata* exhibits a high degree of adaptability, thriving in both wetland and specific dryland habitats. Primarily, the snail feeds on a variety of bright green and succulent aquatic or semiaquatic plants, including duckweed, young rice (*Oryza sativa* L.) seedlings, lotus root, and other small plants that float on the surface of water. When *P. canaliculata* snails infest rice paddy fields with young seedlings, they feed voraciously on the rice plants, which results in significant crop losses if suitable alternative food sources are unavailable. Their extensive invasion into rice paddy fields, through irrigation canals and rivers, may not only devastate the crops but also out-compete native local snails [3,4], potentially altering the normal function of natural ecosystems [5–7].

Flooded rice paddy fields offer a habitat for *P. canaliculata* snails, allowing them to thrive and reproduce rapidly. The water depth in the flooded rice paddy field has a crucial influence on the movement and feeding activities of *P. canaliculata* snails. Research has shown that during the early growth stage of rice (specifically for young seedlings between 21 and 40 days after emergence), if they are submerged in water deeper than 5 cm,

the damage caused by *P. canaliculata* ranges from 46% to 100% [8]. Among the suggested strategies for preventing damage to young seedlings of both direct-seeded and transplanted rice, drainage or maintaining shallow water before the V5 growth stage [9,10], mechanical control through tillage and puddling [11,12], chemical control, crop rotation, and biological control [13] are considered effective.

Nonetheless, maintaining a shallow water level, for example, a level not exceeding 4 cm [14], is not straightforward because most paddy fields are not perfectly level. Water depth varies across the paddy field due to differences in ground elevation; some areas are higher and others are lower, and the elevation throughout the paddy field is generally uneven. Given that areas near water inlets and outlets tend to be deeper, local chemical treatments for these areas are often employed by farmers. However, this method often focuses on addressing limited areas, leaving untreated areas further from the field's access points. Comprehensive chemical treatments for the entire paddy field are also feasible, but are associated with high costs. Therefore, treating only the areas with deep water in the paddy field is a sensible approach.

Water depth data in a paddy field can be obtained by installing sensors at fixed points to measure the water level [15,16]. However, this method can only capture localized data points; it is incapable of providing comprehensive water depth data for the entire field. Obtaining accurate water depth distribution data becomes extremely challenging when the paddy field is flooded with seedlings or there is debris on the flat-water surface. As an alternative, measuring the ground height of the rice paddy when it is not flooded and estimating the water depth during irrigation is a more practical approach. There are currently many highly useful technologies that can be applied to measure bare ground elevation (also known as assessing ground or soil surface elevation). The assessment of ground surface elevation typically follows the criteria recommended for rice paddy fields, indicating an elevation difference within $\pm$5 cm or $\pm$3.5 cm from the mean horizontal plane [17] or an elevation standard deviation below 2 cm [18].

It is challenging to achieve ground surface elevation data with centimeter level precision; traditional methods involving measurements at multiple points, such as Total Stations, theodolites, or Global Navigation Satellite System (GNSS) receivers, may result in missing or incomplete data for unmeasured locations within the designated paddy field. The recent advanced measurement methods that can be adapted to assess ground surface elevation in paddy fields include Terrestrial Laser Scanning (TLS), Unmanned Aerial Vehicle (UAV)-based Light Detection and Ranging (LiDAR), and UAV-based photogrammetry [19,20]. Although TLS technology has proven effective in various applications, such as topographic mapping, architectural documentation, and cultural heritage preservation [21], it exhibits limitations when applied to relatively broad and flat rice paddies, including uneven data density arising from the lack of distinct topographical features, significant time and cost requirements, and the challenge of establishing suitable measurement points during the scanning process. UAV-based LiDAR is well-suited to assessing forest structure [22] or crop height [23–25]. However, when mapping relatively flat terrain, UAV-based photogrammetry is a more advanced choice owing to its cost-effectiveness, outstanding flexibility, and high-resolution. By utilizing high-resolution aerial imagery with accurate Real-Time Kinematic (RTK)-GNSS geo-positioning, UAV-based photogrammetry can achieve measurement accuracy within several centimeters by referencing Ground Control Points (GCPs) [26,27].

Owing to its ability to measure ground elevation differences to within a few centimeters, UAV-based photogrammetry can be applied to our approaches for controlling *P. canaliculata* snails in paddy fields. After the water depth has been estimated from the measured ground elevation data, site-specific application or variable rate (VR) pesticide application [28] can be implemented to save time and reduce costs. In precision agriculture, site-specific application, VR pesticide application, and VR fertilizer application are common practices that tailor input and usage to achieve desired outcomes based on timely diagnosis information on crop growth and the surrounding environment [29]. VR applications are typically performed with reference to the diagnostic information acquired from an on-board

sensor or a prescription map calculated from vegetation indices (VIs) such as the Normalized Difference Vegetation Index (NDVI) [30,31]. For example, based on UAV-derived Green NDVI (GNDVI), Yi et al. [32] used variable rate spraying for cotton defoliation applications. Another valuable indicator for representing ground elevation or crop height, the Digital Surface Model (DSM), has been applied in site-specific applications for orchards or terrains with significant height variations [33]. However, owing to limitations in the accuracy of elevations determined using UAV-based methods, no research has explored the use of DSM indicators to identify and select areas with subtle differences, such as of a few centimeters, for targeted treatments in rice paddy fields.

Building upon insights gained from advanced UAV-based techniques, our study takes a further step by proposing a comprehensive approach that leverages these techniques to enhance the monitoring and prevention of *P. canaliculata* in rice paddy fields. We focus on three key aspects: (1) developing a UAV-based method to assess the field levelness and estimate water depth, enabling the accurate identification of areas prone to snail infestation; (2) implementing site-specific pesticide application based on a prescription map, allowing precise targeting of snail populations while minimizing pesticide usage; and (3) employing UAV-derived imagery analysis to assess and quantify the extent of damage caused by *P. canaliculata* in rice paddy fields. These contributions aim to enhance the efficiency and effectiveness of pest management strategies and ultimately reduce the economic and ecological impacts of *P. canaliculata* in rice production.

2. Materials and Methods

2.1. Study Site

The study site is situated in the northwest of Kyushu, southern Japan, specifically in the Saga Plain. Over the past decade, the average annual temperature in this area is 17.4 degrees Celsius, as derived from historical weather data collected by an automated meteorological data acquisition system near the study site. Owing to the suitable climate and fertile soil, agricultural practices in this area often involve a double-cropping system, with wheat or barley cultivated in the winter and rice or soybeans in the summer. *P. canaliculata* thrives in the summer paddy fields; in the winter, the climate is conducive to a proportion of snails successfully overwintering in the paddy fields [34].

P. canaliculata (Figure 1a–d) becomes active following the transplantation of rice, typically in mid to late June in this double-cropping system period, causing damage to rice seedlings for approximately two weeks. During the machinery-based transplanting process, an insecticide known as Sukuminon, which contains 10.0% metaldehyde, is commonly applied to prevent the damage caused by *P. canaliculata*. This insecticide provides effective control for a period of approximately one week. However, following this period, the efficacy of the insecticide weakens and gradually diminishes; then, combined with historically abundant rainfall during this season, the snails swiftly invade rice paddies through agricultural waterways, channels, and rivers. This rapid invasion leads to destructive damage in rice fields where the protective effect of the insecticides is diminished, which particularly impacts young seedlings (Figure 1e).

Our experimental fields were selected within the high-damage zones caused by *P. canaliculata* snails at the study site, divided into three groups (G_1, G_2, and G_3), with each group containing two paired rice paddies, labeled as follows: F_1 and F_2, F_3 and F_4, F_5, and F_6 (Figure 2). The two paddies in the same group were situated in close geographical proximity; the environmental conditions for rice growth and cultivation practices were identical. Traditional *P. canaliculata* management practices, which involve plowing, puddling, and transplanting with the simultaneous application of the insecticide Scuminon, were carried out in all experimental paddies. The paired paddies in each group were designated as controls: one underwent timely treatment by drone-based application; the other followed traditional management practices in which the initial insecticide was only applied during the transplanting process. Detailed information about the experimental fields is provided in Table 1.

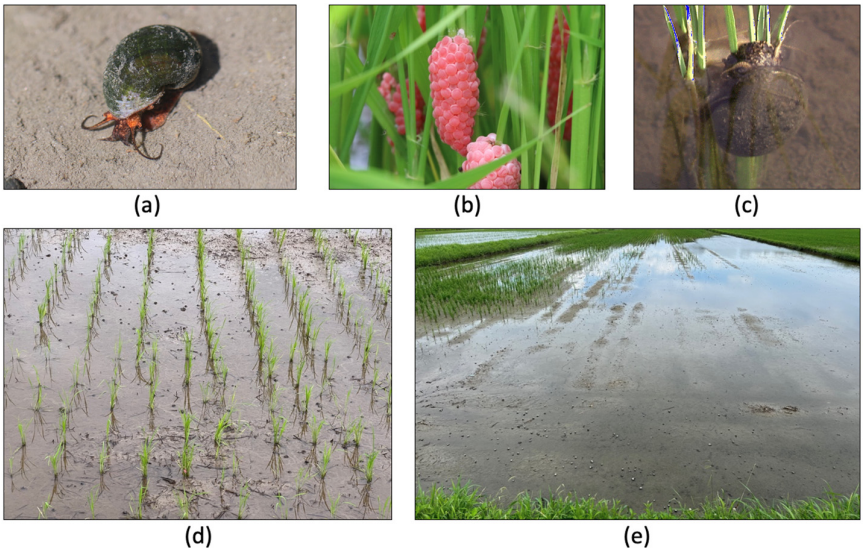

Figure 1. *P. canaliculata* snails. (**a**) Snails inhabiting the paddy field (shell height mostly ranging from 0.3 to 3 cm). (**b**) Egg masses—strong reproductive ability, with annual egg production ranging from 2000 to 8000. (**c**) Snail damage to rice plants. (**d**) Shallow water management at approximately 1 cm depth for paddy fields infested by the snails. (**e**) Significant seedling losses in a paddy field infested with the snails.

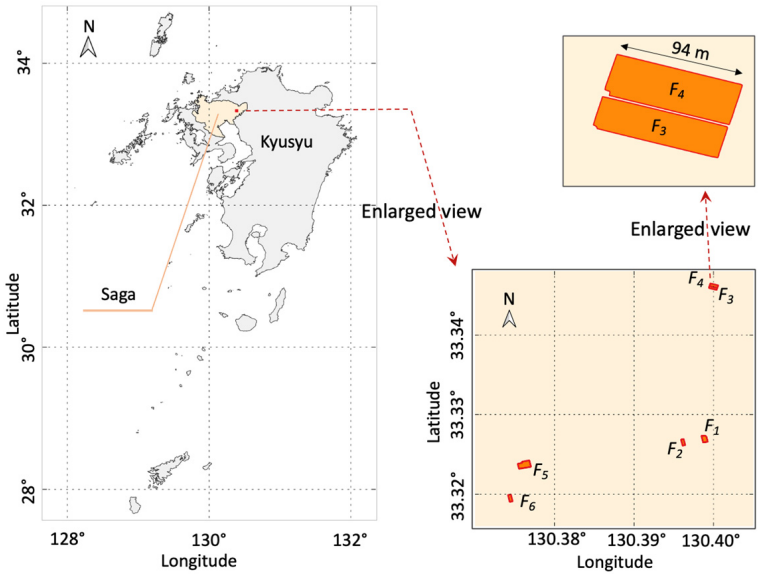

Figure 2. Map of the experimental fields.

Table 1. Information on the experimental fields.

Group	G_1		G_2		G_3	
Field	F_1	F_2	F_3	F_4	F_5	F_6
Area (ha)	0.49	0.26	0.26	0.33	1.18	0.33
Latitude, longitude	33.326974 N 130.398870 E	33.326546 N 130.396180 E	33.345911 N 130.399962 E	33.346190 N 130.400063 E	33.323753 N 130.376322 E	33.319522 N 130.374446 E
Transplanting date	26 June 2023	26 June 2023	24 June 2023	24 June 2023	22 June 2023	23 June 2023
Timely treatment	drone application	-	drone application	-	drone application	-

2.2. UAVs and Agricultural Drones

To estimate the water depth in the experimental fields, we utilized an RTK-UAV, specifically the Phantom 4 RTK (DJI, China). This UAV is equipped with an on-board RGB camera capable of capturing high-resolution images at 4864 × 3648 pixels, ensuring a spatial resolution of 2.7 cm Ground Sampling Distance (GSD) when photographs are taken at an altitude of 100 m Above Ground Level (AGL). The UAV exhibits high positioning accuracy, with a vertical precision of 1.5 cm and horizontal accuracy of 1 cm specified by the manufacturer.

The UAV flight experiment, when the RTK system was in a fixed state, was conducted on 7 June 2023, subsequent to the plowing process that occurred after the harvest of wheat or barley and prior to the puddling. Flight parameters were configured using the DJI GS Pro application, with a flight altitude of 100 m AGL, 75% overlap in both forward and side directions, and a capture mode of 3-s intervals. The weather conditions were clear, with a wind speed below 1 m/s.

The selection of the flight altitude of 100 m AGL is primarily due to its capability to ensure accuracy within a few centimeters in both horizontal and vertical directions, particularly in the flat terrain of lowland rice production areas. According to a review [35], flying the UAV at a higher altitude can significantly improve vertical accuracy over flat terrain, a finding that is similarly corroborated by our previous field experiments [36]. With appropriate methods, it is even feasible to generate an orthomosaic without the need for GCPs [36]. Furthermore, flying at this altitude facilitates efficient surveying, making it suitable for practical large-scale paddy field measurements. Considering the typical row spacing of 30 cm and seedling spacing of 20–25 cm in conventional rice cultivation, the resulting GSD of 2.7 cm at this altitude is adequate for distinguishing individual rice plants, especially for discerning rice canopy from the original images and RGB orthomosaic.

Another flight experiment, executed with the same UAV and settings, was planned and performed on 23 August 2023, approximately 1 week before the rice heading stage. During the flight, the weather conditions were mostly cloudy, with an approximate wind speed of 1.5 m/s.

In our experimental fields dedicated to controlling *P. canaliculata* snails, we opted for Sukumin Bait 3, a granular eradicator containing 3.0% iron (II) phosphate hydrate, with no specific restrictions on application periods or frequency. The granule materials were dispersed from the air using two models of agricultural drones: Nileworks Nile-JZ (Tokyo, Japan) and DJI Agras T10 (Shenzhen, China). The Nile-JZ drone has a maximum takeoff weight of 27 kg, featuring six propellers, an internal load capacity of 8 kg for granule spreading, and achieves a spreading width of over 5 m. The Agras T10 drone, with a maximum takeoff weight of 24.8 kg and four propellers, is equipped with an internal load capacity of 10 kg for granule spreading and achieves a spreading range of 5 to 7 m.

The experimental conditions for aerial spreading are detailed in Table 2. During fixed RTK states, both the Nile-JZ and Agras T10 drones executed automatic spreading operations following predesigned flight routes, including automatic takeoff, spreading along the predetermined paths, and automatic landing. The flight altitudes were set at 1.5 m for Nile-JZ and 2 m for Agras T10, which corresponded to the height of the paddy field ridges and the height from the takeoff point, respectively. It should be noted that the implementation date for the drone-based insecticide application on F_5 preceded F_1 and F_3 by a week due to the earlier transplanting date in field F_5.

Table 2. The experimental conditions for air spreading.

Drone Model	 **Nile-JZ**	 **Agras T10**
Target fields	F_1 and F_3	F_5
Application date	6 July 2023	29 June 2023
Weather	Sunny	Shower
Wind speed (m/s)	4.5	5
Wind direction	SSE	SSW
Temperature (°)	31.7	28.6

2.3. The Research Methodology

Figure 3 illustrates a block diagram of our research methodology; the right-hand column indicates the corresponding instruments and tools used. The research methodology comprises:

- Data acquisition, specifically for aerial images using the RTK-UAV.
- Automated Data Processing (ADP), developed with the Python language and PIX4D engine SDK 1.4 [37]. This includes procedures such as inputting aerial images, generating orthomosaics and the DSM, clipping the DSM of the field, calculating the areas for spreading, and creating the prescription map. The DJI Terra software, not in the procedures for ADP, was used for creating the prescription map for Agras T10.
- Drone flight plan, automatically generated by the Nile app and DJI Terra for their corresponding drone models.
- Drone application, carried out by Nile-JZ or Agras T10.
- Assessment of the damage rate caused by *P. canaliculata* snails, determined from the aerial images acquired by the RTK-UAV.

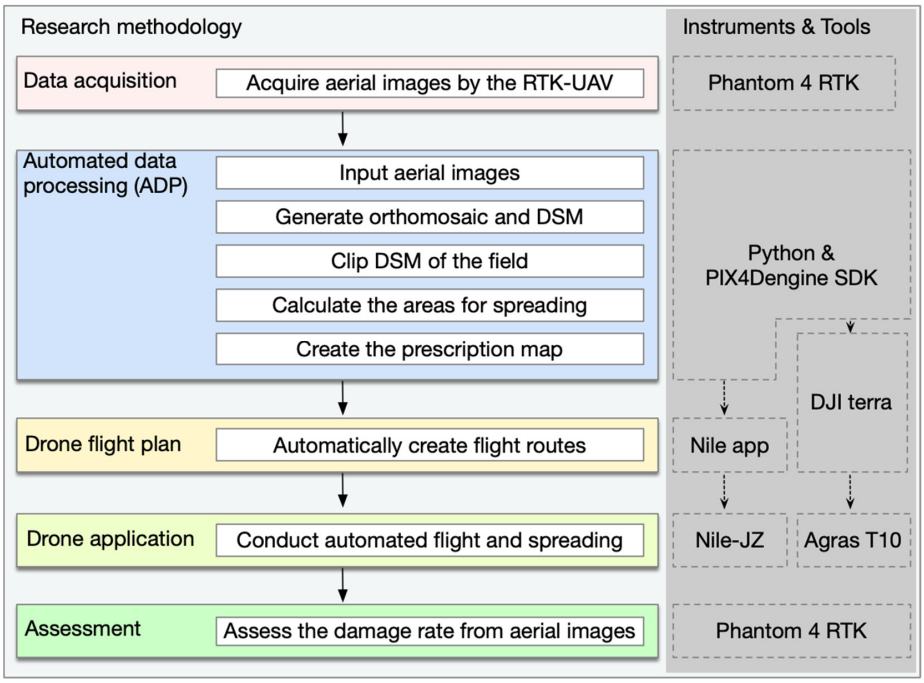

Figure 3. The research methodology, instruments, and tools.

ADP was developed using Python 3.8 on a Windows 10 Pro, 64-bit operating system. The development environment was a high-performance PC equipped with an Intel Xeon(R) Silver 4208 (2.1 GHz, 8 cores), 48 Gb of RAM, and a graphics accelerator with 3328 CUDA cores (NVIDIA RTX A2000, 12 Gb). In addition to PIX4Dengine SDK, the implementation utilized open-source tools such as GDAL/OGR 3.3.2 [38]. PIX4Dengine SDK offered a flexible interface for customizable configurations and processing controls, largely encompassing the capabilities found in PIX4D Mapper Pro, a Structure from Motion (SfM) [39] software developed by the same provider.

After completing aerial imagery acquisition using RTK-UAV at the study site, we obtained a set of images with precise geographical coordinates to serve as the input data for ADP. To better differentiate ground elevation within the same rice paddy, we established predefined geographical boundaries for each of our experimental fields, excluding boundary ridge areas with significant variations in ground elevation that differed from the base ground elevation of the rice paddy. Subsequently, we imported this dataset into ADP for automated processing.

The prescription map, provided in vector data formats such as GeoJSON or ESRI Shapefile by ADP, can be easily imported into Nile app to create optimized flight routes for Nile-JZ. However, DJI Terra, lacking the ability to generate a prescription map based on indices other than NDVI, requires manual referencing to the spreading area.

The assessment of the damage rate caused by P. canaliculata snails is based on the selection of geographical pixels according to the $\frac{R}{G}$ and $\frac{B}{G}$ ratios [40], along with the excess G index [41,42], where R, G, and B denote red, green, and blue digital values ranging from 0 to 255, respectively, in the RGB orthomosaic generated from the RTK-UAV-derived aerial imagery. The assessment was conducted using the following formulas:

$$C = \begin{cases} 1 \textbf{ if } \left(\frac{B}{G} < \theta_1\right) \textbf{ and } \left(\frac{R}{G} < \theta_2\right) \textbf{ and } (2 \times G - R - B \ > \theta_3) \\ 0 \textbf{ otherwise} \end{cases} \quad (1)$$

$$r = \frac{\textbf{sum } (C)}{\textbf{count } (C)} \quad (2)$$

where r represents the canopy cover rate of rice areas, and the threshold values θ_1, θ_2, and θ_3 were determined using the following procedure:

01: **begin**
02: Set the sample size n
03: Extract a set of points P_n from within rice canopy regions
04: Extract a set of points Q_n from outside rice canopy regions
05: Calculate the values of $\frac{R}{G}$, $\frac{B}{G}$ and $2 \times G - R - B$ for each point in P_n and Q_n using a GIS program or tool
06: Assign the 97.5th percentile value of $\frac{R}{G}$ within P_n to θ_1
07: Assign the 97.5th percentile value of $\frac{B}{G}$ within P_n to θ_2
08: Assign the 2.5th percentile value of $2 \times G - R - B$ within P_n to θ_{3a}
09: Filter a subset Q' of points from Q_n with the filter $\frac{R}{G} < \theta_1$ and $\frac{B}{G} < \theta_2$
10: Calculate the 2.5th percentile value θ_{3b} for $2 \times G - R - B$ within Q'
11: Choose the value for θ_3 as the maximum of θ_{3a} and θ_{3b}
12: **end**

In our study, with a sample size of 34, the values of θ_1, θ_2, and θ_3 were determined as 0.82, 0.82, and 60, respectively. These values are subject to variation based on changes in the sample size and sampling points, particularly at critical points between the rice canopy and water surface. To mitigate noise associated with these critical points, values for θ_3 were selected at the 97.5th and 2.5th percentiles. The geographical raster file of the rice canopy was calculated using Equation (1) and validated through a comparison with the RGB orthomosaic.

The values of θ_1, θ_2, and θ_3 significantly deviate from the suggested default values of 0.95, 0.95, and 20 in [43]. This variance may be attributed to specific conditions observed in flooded rice paddies and the presence of floating residues. Damage to rice seedlings by *P. canaliculata* snails results in the loss or partial damage of rice seedlings. In the current mechanized rice cultivation system, replanting will not be conducted for the missing parts, leaving these areas blank until harvest. These areas are easily distinguishable from the aerial images at a flight altitude of 100 m AGL. Partially weak or damaged rice seedlings gradually recover and can reach the maximum canopy area around the rice heading stage. During this stage, aerial images are highly effective in distinguishing rice canopy, where non-rice canopy areas consist of either water surfaces or distinctively colored floating residues. Since we can clearly discern rice canopy from aerial images, we opted to substitute the traditional field sampling method for calculating damage rates. Traditional field sampling also faces challenges, such as determining sampling protocols and accurately aligning predetermined sampling points with positions on the aerial RGB orthomosaic. Moreover, due to discrepancies in evaluation criteria, actual field sampling surveys may not necessarily yield accurate actual damage rates.

3. Results

3.1. Implementation of Site-Specific Drone Application

Figure 4a illustrates the visualized ground elevation map generated after completing the procedures of generating orthomosaics and the DSM, along with clipping DSM of the field F_1. This map, which features color grading and 5 cm contours, provides an intuitive representation of the distribution of height differences and offers valuable insights for decision making in insecticide application.

ADP automatically analyzed the histogram of the elevation distribution data. Considering the possibility of increased water levels due to heavy rain, the 95% percentile of these data was considered to be the water level at 0, and values below the threshold (4 cm below the water level [14]) were identified as the points for insecticide application (Figure 4b). Based on this threshold value, areas requiring insecticide application were marked and transformed into a 1 m grid cell map, which is referred to as the prescription map (Figure 4c). The prescription map with a 1 m grid cell is advantageous for creating a flight route with high covering accuracy, particularly concerning the designated area, for agricultural drones. The flight routes for agricultural drones, with maximum effective working width, often require adjustments in flight direction based on on-site factors such as traffic, obstacles, and wind direction. However, the flight direction of the on-site generated grid cell, for example, 5 m $\times$ 5 m, is likely not aligned with the 1 m grid cell direction, leading to errors in the designated spray quantity due to the intersection of grid cells of two different sizes. This error tends to decrease as the grid cell size becomes smaller.

Moreover, the prescription map with a 1 m grid cell broadens the applicability of the data. It can be utilized not only with the Nile-JZ used in this experiment but also with other agricultural drones. Additionally, it is compatible with various agricultural machinery, including boom sprayers, fertilizer applicators, and agricultural helicopters, that adhere to the ISO 11783-10 data interface. This compatibility arises from the fact that the 1 m grid cell has vertical and horizontal directions designated as north and east, aligning with the same orientation as the grid cell defined in ISO 11783-10.

Utilizing the prescription map, Nile-JZ autonomously performed the insecticide application, along with optimized flight paths parallel to the long side of the field, aiming to minimize untreated areas, aligning with the designated areas in the 1 m grid cell on the prescription map. The actual spreading paths (Figure 4d) were plotted from the aircraft log data. It is evident that the aircraft's spreading covered the vast majority of the designated spreading areas. Because the aircraft has a spreading width limitation of 5 m, some of the scattered and small areas indicated for spreading were not treated.

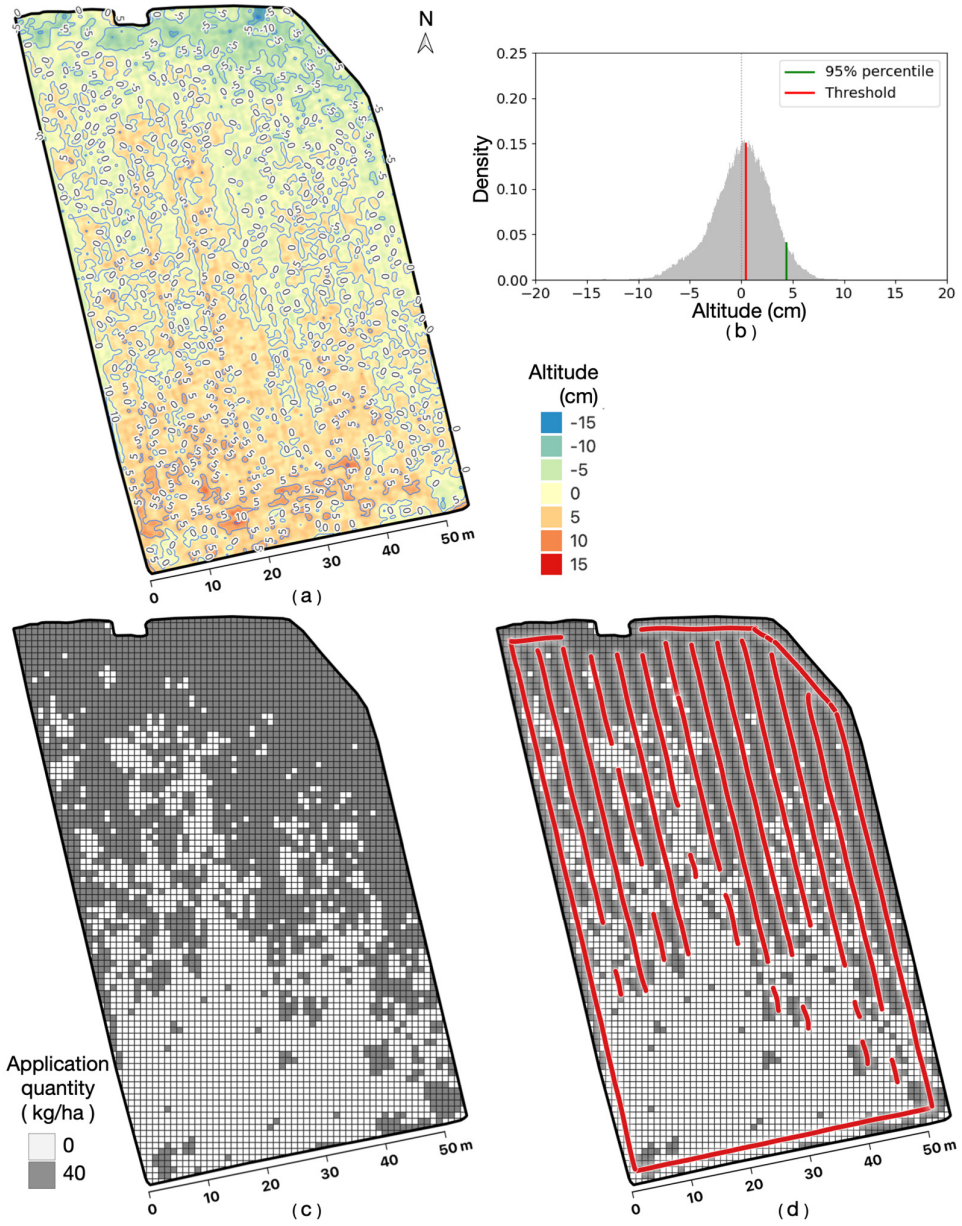

Figure 4. Site-specific drone application based on the prescription map for F_1. (**a**) Visualized ground elevation map with color grading and 5 cm contours. (**b**) Histogram of ground elevation data with a red-line threshold and a green-line 95% percentile. (**c**) Prescription map with 1 m grid cell for application quantity. (**d**) Flight paths indicated by red lines for drone application using Nile-JZ.

The same procedures were applied to F_3. In Figure 5a, the region with higher ground elevation (presented in deep red in the upper-left part) remained unsubmerged during the on-site inspection on the fourth day after transplantation (28 June 2023), whereas the water depth exceeded 15 cm in the lower-right corner. The spreading paths of Nile-JZ (Figure 5c) confirmed that no spreading operations were performed in the areas remaining unsubmerged areas, aligning with expectations.

Owing to various factors, including weather conditions, the optimal spreading implementation time window, and the scheduling of the experimental agenda, a different spreading method was applied for F_5. Agricultural land identification and spreading area settings were manually specified on DJI Terra. Then, the Agras T10 executed continuous and uniform spreading in this area with 40 kg/ha settings (Figure 6b). The red lines of the spreading paths in Figure 6b were manually drawn based on a screenshot from the DJI Agras App, as flight log data were not accessible.

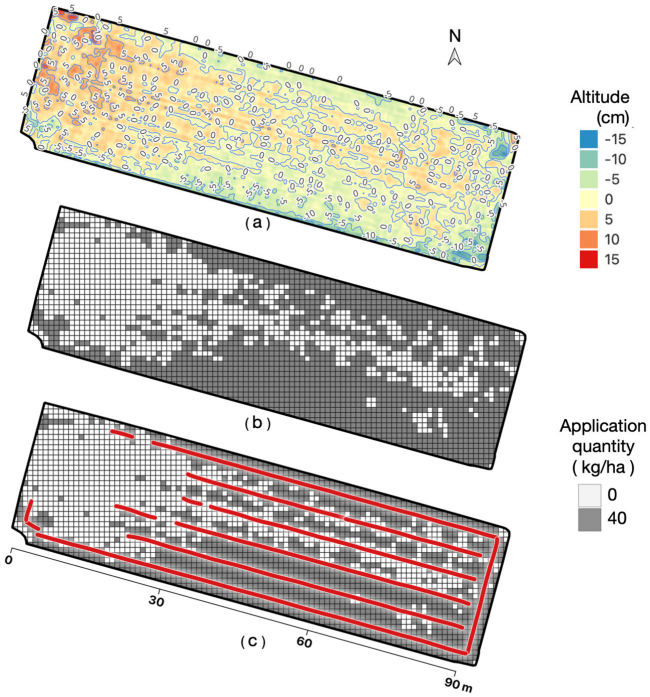

Figure 5. Site-specific drone application based on the prescription map for F_3. (**a**) Visualized ground elevation map with color grading and 5 cm contours. (**b**) Prescription map with 1 m grid c for application quantity. (**c**) Flight paths indicated by red lines for drone application using Nile-JZ.

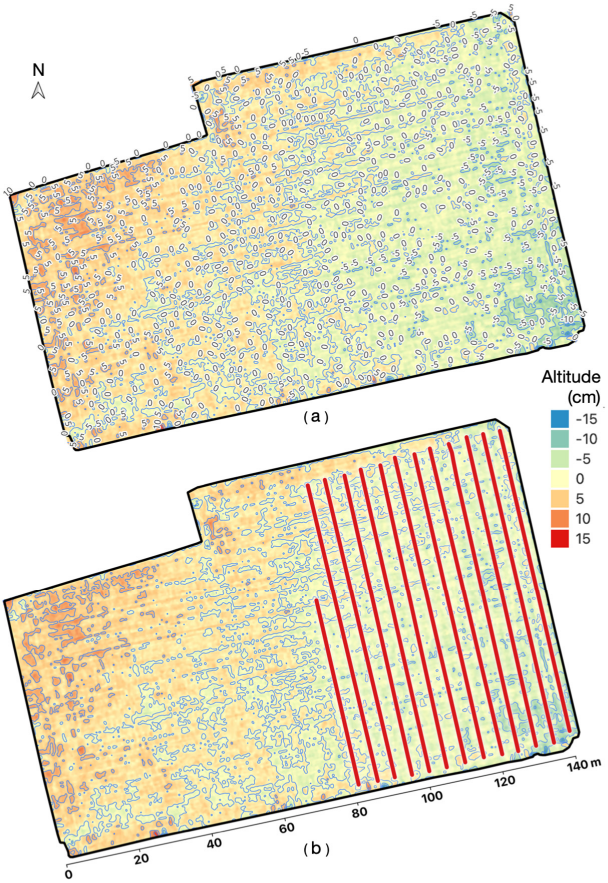

Figure 6. Site-specific drone application based on the prescription map for F_5. (**a**) Visualized ground elevation map with color grading and 5 cm contours. (**b**) Flight paths indicated by red lines for drone application using Agras T10.

3.2. Effectiveness Analysis of Site-Specific Drone Application

The effectiveness of site-specific drone-based insecticide application was assessed approximately 1 week before the rice heading stage. This timeframe was strategically chosen as it provided the optimal evaluation window. At this point, rice plants that had suffered destructive damage were unlikely to recover, and the well-developed branches and leaves would effectively cover normal row and plant spacing. The evaluation process first involved aerial photography and the generation of an RGB orthomosaic. Subsequently, the canopy cover rate was calculated using Equation (1). These results are visualized in Figure 7. In this figure, green represents the canopy cover of rice and white represents areas other than rice, such as water surfaces. It is evident that the canopy cover area on the left side, corresponding to F_1 with drone application, is significantly more than the canopy cover area on the right side, corresponding to F_2 without drone application. This observation implies that the damage rate in F_1, which was subject to drone application, is noticeably lower than in the untreated F_2.

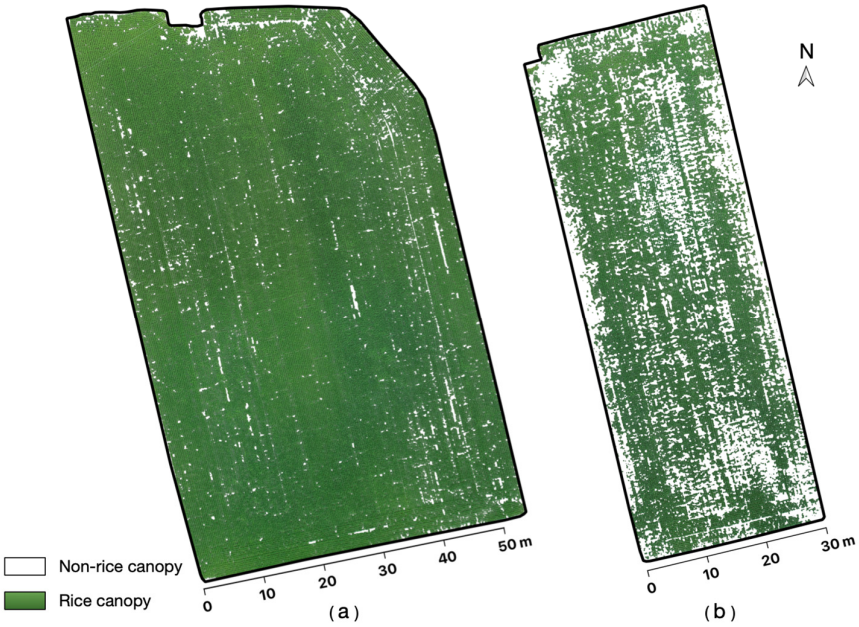

Figure 7. Rice green canopy for estimating damage rates. (**a**) Field F_1 with drone application; (**b**) Field F_2 without drone application.

A comparison of the damage rates in the three control experimental fields is presented in Figure 8a. When comparing damage rates in fields with prescription map-derived drone application (F_1, F_3) to those without drone application (F_2, F_4), the respective rates were 4.0%, 10.8% versus 33.2%, 23.6%. The field area-weighted arithmetic means for the two fields with prescription map-derived drone application and those without were 6.4% and 27.8%, respectively, indicating a difference of 21.4%. For field F_5 with non-prescription map-derived drone application and F_6 without drone application, the respective damage rates were 4.6% and 12.7%, with a difference of 8.1%.

By simultaneously reducing the damage rates, the quantity of insecticide applied through drone application is significantly lower compared with the total field application quantity by traditional uniform application (Figure 8b). For example, in F_1, F_3, and F_5, if traditional uniform application was employed at a rate of 40 kg/ha, the required quantity of chemicals would be 19.6 kg, 10.5 kg, and 47.3 kg, respectively. However, the quantities required for prescription map-derived drone application were 14.0 kg and 7.7 kg for F_1 and F_3, equivalent to reductions of 28.4%, 26.5%, respectively. Similarly, the quantities required for non-prescription map-derived drone application were 19.2 kg, equivalent to reductions of 59.4%.

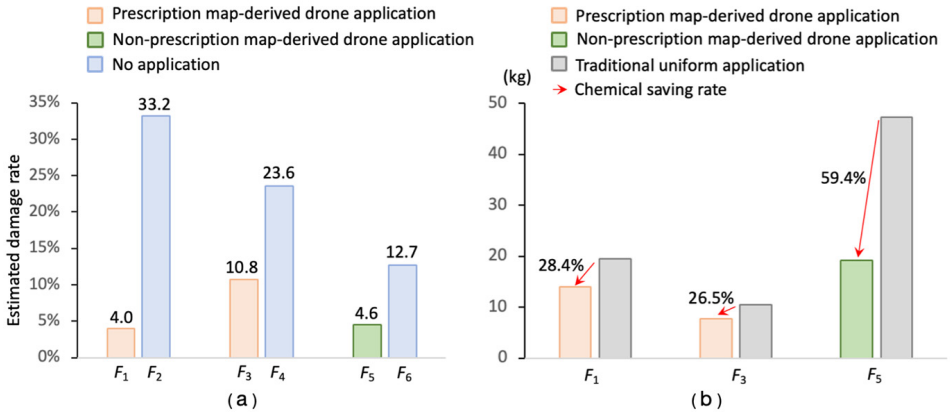

Figure 8. Rates of damage reduction and chemical savings. (**a**) Comparison of estimated damage rates at each field group between drone application and no application; (**b**) Chemical saving rates between total field application quantity by traditional uniform application and drone application.

If we neglect the method of implementing a prescription map in drone application, the field area-weighted arithmetic means for the three fields with drone application and those without application were 5.3% and 22.5%, respectively, which is a difference of 17.2%. This reduction in damage rate is expected to translate into an increase in final yield. Specifically, the yield in rice fields with drone application is anticipated to be 17.2% higher than in fields without application.

4. Discussion

This study utilized UAV-based sensing technologies to identify areas that were highly vulnerable to damage by *P. canaliculata* snails. Subsequently, autonomous agricultural drones were deployed to perform precise and efficient site-specific applications in these identified regions. In comparison with the traditional control approaches, this method not only mitigated damage rates but also reduced chemical usage. The accuracy in identifying areas at high risk of damage is pivotal for the success of the prescription map for drone-based applications. The precision of UAV-based DSM, portraying the ground elevation surface of rice paddies, is thus indispensable for the generation of prescription maps. In this study, we obtained highly precise DSM using the methods outlined in [29], which encompassed (1) conducting UAV flights at an altitude of 100 m AGL or higher during stable weather conditions and (2) achieving high-quality camera calibration during the orthomosaic generation process. If the quality in the orthomosaic generation report was suboptimal, calibration with GCPs is recommended.

It is essential to note that the time window available for drone sensing in double-cropping systems is not large. For transplanting rice, it is performed following the plowing process after the harvest of winter crops (such as wheat or barley) and before puddling. In the case of direct-seeded rice, it is advisable to conduct the operation before or around the germination period, preferably before the V3 growth stage to mitigate noise caused by water surfaces or young rice plants. Equally important is the correct weather conditions during UAV sensing; non-rainy days with ground wind speeds below 5 m/s are favored.

The generation of the prescription map is automated by ADP due to the utilization of PIX4Dengine SDK during orthomosaic and DSM creation. In addition to its capabilities for automatic processing, PIX4Dengine SDK can be extended to accommodate applications, including *P. canaliculata* control. Alternatively, standalone SfM software can also be used, but after obtaining the orthomosaic and DSM, manual tasks are required, such as clipping the DSM of the field, calculating thresholds for spreading areas, and conversion into a 1 m grid cell map.

As mentioned in [44], there is still a paucity of research on agriculture drone-based site-specific or variable rate applications, which is primarily attributable to the limited availability of drone models capable of such precise application. Furthermore, prescription

maps, while frequently grounded on NDVI indices or yield maps, might instead encompass more useful indices, such as other VIs or DSM. The selection of agricultural drones that support prescription maps created with DSM, such as Nile-JZ, or prescription maps in a universal format, is a prerequisite for the successful implementation of the technology in our study.

In the study, we did not conduct an actual yield survey because, in areas where rice is completely missing with no rice plants, the yield is naturally zero. In areas where rice is not missing, the number of rice plants does not necessarily equate to the damage rate, as yield can be influenced by individual differences in rice plants. Instead, we calculated potential yield losses based on the damage rate. Furthermore, we did not assess the final profits derived from our research methodology. Profit calculations would need to consider various other influencing factors, such as material and equipment costs, software expenses, development costs, and labor costs, which were beyond the scope of our study. Opting only for simple profit data based on increased yield and cost savings in pesticides may be feasible but lacks representativeness and persuasiveness, especially in the absence of exact yield data.

Currently, we are in the process of developing another study that comprehensively evaluates the practical operational benefits of using our research methodology, taking into account a wide range of factors. Additionally, our ongoing future works include: (1) attempting to expand the time window available for UAV-based sensing in double-cropping systems to alleviate the compression of intensive operations during rice transplantation; and (3) developing a public data interface for prescription maps in agricultural drones and applying it to other pest control or variable rate application scenarios.

5. Conclusions

Our study has established that site-specific drone-based insecticide application is a viable and efficient strategy for mitigating damage to rice paddies by *P. canaliculata*. The high precision of the prescription map, derived from RTK-UAV-based aerial imagery, provides accurate site-specific application guidance to facilitate efficient treatment precisely where needed. The automated data processing involved in generating the prescription map streamlines the postprocessing of raw aerial images, improving processing efficiency and reducing technological barriers for general farmers. The implementation of site-specific applications by two autonomous agricultural drones was able to achieve noticeable reductions in damage rates and chemical usage, showing the potential to increase yield and improve the sustainability of agricultural practices. These findings, which contribute to the advancement of precision agriculture, underscore the importance of considering topographical variations, including subtle changes at the centimeter level, in pest control strategies.

Author Contributions: S.G., conceptualization, methodology, investigation, software, validation, and writing—original draft preparation, review, and editing; K.T. (Kimiyasu Takahashi), conceptualization, methodology, project administration, investigation, supervision, funding acquisition, and writing—review. S.W., software, investigation, resources, and writing—review; K.T. (Katsunori Tanaka), project administration, investigation, resources, funding acquisition, and writing—review. All authors have read and agreed to the published version of the manuscript.

Funding: This research was partly supported by "Research project for technologies to strengthen the international competitiveness of Japan's agriculture and food industry" Shin1do1 (21452858) and the Research Program on Development of Innovative Technology grants (JPJ007097) from the Bio-oriented Technology Research Advancement Institution (BRAIN).

Data Availability Statement: The data presented in this study are available on request from the corresponding author.

Acknowledgments: Sincere thanks are extended to Akitoshi Honbu, Makoto Nakajima, and Atsuya Yokota for their contributions to data acquisition in both the field survey experiment and UAV photogrammetry. Gratitude is also extended to Agribase Niiyama Ltd. for generously providing access to experimental fields and necessary resources. The authors would like to express special thanks to Masumi Kabashima for her diligent efforts in programming and assisting with data processing for this research.

Conflicts of Interest: Author Shunichiro Watanabe and Katsunori Tanaka were employed by the company Nileworks Co., Ltd. 2F. The authors declare that this study received fundings from "Research project for technologies to strengthen the international competitiveness of Japan's agriculture and food industry" Shin1do1 (21452858) and the Research Program on Development of Innovative Technology grants (JPJ007097) from the Bio-oriented Technology Research Advancement Institution (BRAIN). The funders were not involved in the study design, collection, analysis, interpretation of data, the writing of this article or the decision to submit it for publication.

Abbreviations

The following abbreviations are used in this manuscript:

ADP	Automated Data Processing
AGL	Above Ground Level
DSM	Digital Surface Model
GCP	Ground Control Point
GNSS	Global Navigation Satellite System
GSD	Ground Sample Distance
GNDVI	Green Normalized Difference Vegetation Index
LiDAR	Light Detection and Ranging
NDVI	Normalized Difference Vegetation Index
RTK	Real-Time Kinematic
TLS	Terrestrial Laser Scanning
UAV	Unmanned Aerial Vehicle
VR	Variable Rate

References

1. Lowe, S.; Browne, M.; Boudjelas, S.; De Poorter, M. *100 of the World's Worst Invasive Alien Species: A Selection from the Global Invasive Species Database*; Invasive Species Specialist Group: Auckland, New Zealand, 2000; Volume 12.
2. CABI Digital Library. Pomacea canaliculata (Invasive Apple Snail). 2013. Available online: https://www.cabidigitallibrary.org/doi/10.1079/cabicompendium.68490 (accessed on 21 June 2023).
3. Halwart, M. The golden apple snail *Pomacea canaliculata* in Asian rice farming systems: Present impact and future threat. *Int. J. Pest Manag.* **1994**, *40*, 199–206. [CrossRef]
4. Chaichana, R.; Sumpan, T. The potential ecological impact of the exotic snail *Pomacea canaliculata* on the Thai native snail Pila scutata. *Sci. Asia* **2014**, *40*, 11–15. [CrossRef]
5. Carlsson, N.; Kestrup, Å.; Mårtensson, M.; Nyström, P. Lethal and non-lethal effects of multiple indigenous predators on the invasive golden apple snail (*Pomacea canaliculata*). *Freshw. Biol.* **2004**, *49*, 1269–1279. [CrossRef]
6. Carlsson, N.O.; Brönmark, C.; Hansson, L.A. Invading herbivory: The golden apple snail alters ecosystem functioning in Asian wetlands. *Ecology* **2004**, *85*, 1575–1580. [CrossRef]
7. Joshi, R. Problems with the management of the golden apple snail *Pomacea canaliculata*: An important exotic pest of rice in Asia. In *Area-Wide Control of Insect Pests: From Research to Field Implementation*; Springer: Dordrecht, The Netherlands, 2007; pp. 257–264.
8. Sin, T.S. Damage potential of the golden apple snail *Pomacea canaliculata* (Lamarck) in irrigated rice and its control by cultural approaches. *Int. J. Pest Manag.* **2003**, *49*, 49–55. [CrossRef]
9. Wada, T.; Ichinose, K.; Higuchi, H. Effect of drainage on damage to direct-sown rice by the apple snail *Pomacea canaliculata* (Lamarck)(Gastropoda: Ampullariidae). *Appl. Entomol. Zool.* **1999**, *34*, 365–370. [CrossRef]
10. Counce, P.A.; Keisling, T.C.; Mitchell, A.J. A uniform, objective, and adaptive system for expressing rice development. *Crop Sci.* **2000**, *40*, 436–443. [CrossRef]
11. Takahashi, K.; Seki, M.; Nishida, H. Prevention of the Harm from Apple Snail with Rotary Cultivator. *J. Jpn. Soc. Agric. Mach.* **2002**, *64*, 101–107. [CrossRef]
12. Takahashi, K.; Seki, M.; Higashi, S.; Miike, T. Development of Technology by Rotary Tiller to Control the Density of Apple Snail. *J. Jpn. Soc. Agric. Mach.* **2005**, *67*, 68–74. [CrossRef]
13. Wada, T. Strategies for Controlling the Apple Snail *Pomacea canaliculata* (Lamarck) (Gastropoda: Ampullariidae) in Japanese Direct-Sown Paddy Fields. *Jpn. Agric. Res. Q. JARQ* **2004**, *38*, 75–80. [CrossRef]

14. Makiyama, M.; Itoh, T. The Effects of Shallow Ponding Depth for Control of the Damage by *Pomacea canaliculata*. *J. Agric. Eng. Soc. Jpn.* **2005**, *73*, 793–796. [CrossRef]
15. Kawakami, Y.; Furuta, T.; Nakagawa, H.; Kitamura, T.; Kurosawa, K.; Kogami, K.; Tajino, N.; Tanaka, M.S. Rice cultivation support system equipped with water-level sensor system. *IFAC-PapersOnLine* **2016**, *49*, 143–148. [CrossRef]
16. Cruz, K.M.S.D.; Ella, V.B.; Suministrado, D.C.; Pereira, G.S.; Agulto, E.S. A Low-Cost Wireless Sensor for Real-Time Monitoring of Water Level in Lowland Rice Field under Alternate Wetting and Drying Irrigation. *Water* **2022**, *14*, 4128. [CrossRef]
17. Osari, H. A method for assessing land leveling to produce high-quality consolidated paddy fields. *Paddy Water Environ.* **2003**, *1*, 35–41. [CrossRef]
18. Yamaji, E. Standard and evaluation of paddy field consolidation. In Proceedings of the Soil and Water Engineering for Paddy Field Management, International Workshop, Bangkok, Thailand, 28–30 January 1992.
19. Mora, O.E.; Suleiman, A.; Chen, J.; Pluta, D.; Okubo, M.H.; Josenhans, R. Comparing sUAS photogrammetrically-derived point clouds with GNSS measurements and terrestrial laser scanning for topographic mapping. *Drones* **2019**, *3*, 64. [CrossRef]
20. Rivera, G.; Porras, R.; Florencia, R.; Sánchez-Solís, J.P. LiDAR applications in precision agriculture for cultivating crops: A review of recent advances. *Comput. Electron. Agric.* **2023**, *207*, 107737. [CrossRef]
21. Ulvi, A. Documentation, Three-Dimensional (3D) Modelling and visualization of cultural heritage by using Unmanned Aerial Vehicle (UAV) photogrammetry and terrestrial laser scanners. *Int. J. Remote Sens.* **2021**, *42*, 1994–2021. [CrossRef]
22. Wallace, L.; Lucieer, A.; Malenovský, Z.; Turner, D.; Vopěnka, P. Assessment of forest structure using two UAV techniques: A comparison of airborne laser scanning and structure from motion (SfM) point clouds. *Forests* **2016**, *7*, 62. [CrossRef]
23. ten Harkel, J.; Bartholomeus, H.; Kooistra, L. Biomass and crop height estimation of different crops using UAV-based LiDAR. *Remote Sens.* **2019**, *12*, 17. [CrossRef]
24. Sofonia, J.; Shendryk, Y.; Phinn, S.; Roelfsema, C.; Kendoul, F.; Skocaj, D. Monitoring sugarcane growth response to varying nitrogen application rates: A comparison of UAV SLAM LiDAR and photogrammetry. *Int. J. Appl. Earth Obs.* **2019**, *82*, 101878. [CrossRef]
25. Maimaitijiang, M.; Sagan, V.; Erkbol, H.; Adrian, J.; Newcomb, M.; LeBauer, D.; Pauli, D.; Shakoor, N.; Mockler, T. UAV-based sorghum growth monitoring: A comparative analysis of lidar and photogrammetry. *ISPRS Ann. Photogramm. Remote Sens. Spat. Inf. Sci.* **2020**, *3*, 489–496. [CrossRef]
26. Urban, R.; Reindl, T.; Brouček, J. Testing of drone DJI Phantom 4 RTK accuracy. In *Advances and Trends in Geodesy, Cartography and Geoinformatics II*; CRC Press: Boca Raton, FL, USA, 2020; pp. 99–105.
27. Ekaso, D.; Nex, F.; Kerle, N. Accuracy assessment of real-time kinematics (RTK) measurements on unmanned aerial vehicles (UAV) for direct geo-referencing. *Geo Spat. Inf. Sci.* **2020**, *23*, 165–181. [CrossRef]
28. Swinton, S.; Lowenberg-DeBoer, J. Evaluating the profitability of site-specific farming. *J. Prod. Agric.* **1998**, *11*, 439–446. [CrossRef]
29. Bongiovanni, R.; Lowenberg-DeBoer, J. Precision agriculture and sustainability. *Precis. Agric.* **2004**, *5*, 359–387. [CrossRef]
30. Zhang, J.; Wang, W.; Krienke, B.; Cao, Q.; Zhu, Y.; Cao, W.; Liu, X. In-season variable rate nitrogen recommendation for wheat precision production supported by fixed-wing UAV imagery. *Precis. Agric.* **2022**, *23*, 830–853. [CrossRef]
31. Pawase, P.P.; Nalawade, S.M.; Bhanage, G.B.; Walunj, A.A.; Kadam, P.B.; Durgude, A.G.; Patil, M.G. Variable rate fertilizer application technology for nutrient management: A review. *Int. J. Agric. Biol. Eng.* **2023**, *16*, 11–19. [CrossRef]
32. Yi, L.; Lan, Y.; Kong, H.; Kong, F.; Huang, H.; Han, X. Exploring the potential of UAV imagery for variable rate spraying in cotton defoliation application. *Int. J. Precis. Agric. Aviat.* **2019**, *2*, 42–45. [CrossRef]
33. Wang, C.; Liu, Y.; Zhang, Z.; Han, L.; Li, Y.; Zhang, H.; Wongsuk, S.; Li, Y.; Wu, X.; He, X. Spray performance evaluation of a six-rotor unmanned aerial vehicle sprayer for pesticide application using an orchard operation mode in apple orchards. *Pest Manag. Sci.* **2022**, *78*, 2449–2466. [CrossRef]
34. Yoshida, K.; Wada, T.; Matsukura, K.; Shiba, T. Potential overwintering areas of the alien apple snail, *Pomacea canaliculata*. *Aquat. Invasions* **2022**, *17*, 402–414. [CrossRef]
35. Jiménez-Jiménez, S.I.; Ojeda-Bustamante, W.; Marcial-Pablo, M.D.J.; Enciso, J. Digital terrain models generated with low-cost UAV photogrammetry: Methodology and accuracy. *ISPRS Int. J. Geo-Inf.* **2021**, *10*, 285. [CrossRef]
36. Guan, S.; Takahashi, K.; Nakano, K.; Fukami, K.; Cho, W. Real-Time Kinematic Imagery-Based Automated Levelness Assessment System for Land Leveling. *Agriculture* **2023**, *13*, 657. [CrossRef]
37. PIX4D. *Pix4Dengine SDK Quick-Start*; PIX4D S.A.: Prilly, Switzerland, 2019.
38. GDAL/OGR Contributors. *GDAL/OGR Geospatial Data Abstraction Software Library*; Open Source Geospatial Foundation: Beaverton, OR, USA, 2021.
39. Westoby, M.J.; Brasington, J.; Glasser, N.F.; Hambrey, M.J.; Reynolds, J.M. 'Structure-from-Motion' photogrammetry: A low-cost, effective tool for geoscience applications. *Geomorphology* **2012**, *179*, 300–314. [CrossRef]
40. Paruelo, J.M.; Lauenroth, W.K.; Roset, P.A. Estimating aboveground plant biomass using a photographic technique. *Rangel. Ecol. Manag./J. Range Manag. Arch.* **2000**, *53*, 190–193. [CrossRef]
41. Meyer, G.E.; Neto, J.C. Verification of color vegetation indices for automated crop imaging applications. *Comput. Electron. Agric.* **2008**, *63*, 282–293. [CrossRef]
42. Woebbecke, D.M.; Meyer, G.E.; Von Bargen, K.; Mortensen, D.A. Color indices for weed identification under various soil, residue, and lighting conditions. *Trans. Asae* **1995**, *38*, 259–269. [CrossRef]

43. Patrignani, A.; Ochsner, T.E. Canopeo: A powerful new tool for measuring fractional green canopy cover. *Agron. J.* **2015**, *107*, 2312–2320. [CrossRef]
44. Song, C.; Zhou, Z.; Zang, Y.; Zhao, L.; Yang, W.; Luo, X.; Jiang, R.; Ming, R.; Zang, Y.; Zi, L.; et al. Variable-rate control system for UAV-based granular fertilizer spreader. *Comput. Electron. Agric.* **2021**, *180*, 105832. [CrossRef]